Gap Junctions and Emergent Rhythms

S. Coombes and M. Zachariou

Abstract Gap-junction coupling is ubiquitous in the brain, particularly between the dendritic trees of inhibitory interneurons. Such direct nonsynaptic interaction allows for direct electrical communication between cells. Unlike spike-time driven synaptic neural network models, which are event based, any model with gap junctions must necessarily involve a single neuron model that can represent the shape of an action potential. Indeed, not only do neurons communicating via gaps feel super-threshold spikes, but they also experience, and respond to, sub-threshold voltage signals. In this chapter, we show that the so-called *absolute* integrate-and-fire model is ideally suited to such studies. At the single neuron level voltage traces for the model may be obtained in closed form, and are shown to mimic those of fast-spiking inhibitory neurons. Interestingly, in the presence of a slow spike adaptation current, the model is shown to support periodic bursting oscillations. For both tonic and bursting modes, the phase response curve can be calculated in closed form. At the network level we focus on global gap junction coupling and show how to analyze the asynchronous firing state in large networks. Importantly, we are able to determine the emergence of nontrivial network rhythms due to strong coupling instabilities. To illustrate the use of our theoretical techniques (particularly the phase-density formalism used to determine stability) we focus on a spike adaptation induced transition from asynchronous tonic activity to synchronous bursting in a gap-junction coupled network.

Introduction

Gap-junction coupling is known to occur between many cell types, including for example pancreatic-β cells [13], heart cells [15], astrocytes [6], and neurons [22]. In this latter context, these junctions are primarily found between inhibitory cells

S. Coombes (✉)
School of Mathematical Sciences, University of Nottingham, Nottingham NG7 2RD, UK
e-mail: stephen.coombes@nottingham.ac.uk

K. Josić et al. (eds.), *Coherent Behavior in Neuronal Networks*, Springer Series in Computational Neuroscience 3, DOI 10.1007/978-1-4419-0389-1_5,

[26]. Interestingly, interneurons are known to play a key role in the generation of hippocampal and cortical rhythms, such as those at gamma frequency (30–100 Hz) [9, 21]. Gap junctions allow for the direct electrical communication between cells, and without the need for receptors to recognize chemical messengers are much faster than chemical synapses at relaying signals. The synaptic delay for a chemical synapse is typically in the range 1–100 ms, while the synaptic delay for an electrical synapse may be only about 0.2 ms. There is now little doubt that gap junctions play a substantial role in the generation of neural rhythms [5, 28], both functional [1, 5, 25, 28] and pathological [17, 51]. One natural question therefore is how does the presence of gap-junction coupling affect synchronous neuronal firing [4, 24, 40]. Independent experimental studies have proposed that gaps synchronize neuronal firing even in the absence of chemical synapses [16, 37]. However, other studies have demonstrated that synchrony can result from the interplay of electrical and chemical signaling and that gaps alone are not sufficient for obtaining synchronous activity [7, 47]. Contradictory results have been reported in the case of inspiratory motorneurons, where gaps desynchronize neural activity whereas synaptic inhibition alone promotes synchrony [8]. From a theoretical perspective the theory of weakly coupled oscillators has often been used to understand how gap junction coupling promotes synchrony or antisynchrony depending on the nature of the neural oscillator and the shape of the action potential [18, 31, 32, 35, 36, 41, 42, 46]. By its very nature, however, this sort of approach cannot tackle gap-induced variations in single neuron firing rate and is thus not ideally suited to answering questions about how the strength of gap junctions contributes to coherent neuronal behavior. Thus, we are led to the search for a tractable network model that can be analyzed in the strong coupling limit. In this chapter, we show how one can make progress in the strong coupling regime for a certain class of spiking neuron model that mimics the behavior of fast-spiking interneurons. Importantly, we are able to quantify a transition from asynchronous tonic spiking to synchronized bursting oscillations in a large globally gap-junction coupled network.

The layout of this chapter is as follows. In section "The Absolute Integrate-and-Fire Model," we introduce our single neuron model of choice, namely a nonlinear integrate-and-fire model, with a piece-wise linear nonlinearity. We show that this model can mimic the behavior of a fast-spiking interneuron whilst being analytically tractable. In illustration, we calculate periodic orbits and the phase response curve in closed form. A simple model of spike adaptation is used to augment this basic model so that it can also fire in a burst mode. Next in section "Gap-Junction Coupling," we pursue the analysis of large globally gap-junction coupled networks. The focus here is on asynchronous states that generate a constant mean field signal. These are calculated in closed form and provide the starting point for a subsequent stability analysis. This makes use of ideas originally developed by van Vreeswijk [48] for the study of synaptic interactions. Importantly, we are able to generate the instability borders in parameter space beyond which an asynchronous state is unstable to periodic temporal perturbations. Direct numerical simulations confirm the correctness of our calculations and show that the dominant solution to emerge beyond an instability is one where the mean-field signal shows a classical bursting

signature. Moreover, neurons in this state are synchronized at the level of their firing rate, but not at the level of individual spikes. Finally in section "Discussion," we discuss natural extensions of the work in this chapter.

The *Absolute* Integrate-and-Fire Model

The presence of gap-junctional coupling in a neuronal network necessarily means that neurons directly "feel" the shape of action potentials from other neurons to which they are connected. From a modeling perspective one must therefore be careful to work with single neuron models that have an accurate representation of an action potential shape. On the other hand it is also desirable to work with a model that can be analyzed. A recent paper [12] advocates the use of piece-wise linear planar models. As an alternative we consider here the use of a nonlinear integrate-and-fire (IF) model. Indeed the quadratic IF model is a common choice for computational studies (and unlike the leaky IF model does generate an action potential shape). However for arbitrary time-dependent forcing formal closed solutions are not known. A somewhat overlooked tractable nonlinear IF model is that of Karbowski and Kopell [30], with a voltage dynamics given by

$$\dot{v} = f(v) + I, \tag{1}$$

subject to $v \to v_{\mathrm{r}}$ if $v = v_{\mathrm{th}}$. Here the function $f(v)$ has a shape like $|v - v_{\mathrm{s}}|$ and hence the name *absolute* integrate-and-fire (aif) model, for some *switch* value v_{s}. The firing times T^n, $n \in \mathbb{Z}$, are defined according to

$$T^n = \inf\{t \mid v(t) \geq v_{\mathrm{th}} \,;\, t \geq T^{n-1}\}. \tag{2}$$

Because of the choice of a piece-wise linear form of the nonlinearity, the aif model can be explicitly analyzed. To see that it is capable of generating behavior consistent with that of a fast-spiking interneuron we compare it with a more detailed biophysical model. A generic model for a neocortical fast-spiking interneuron is that of Wang and Buzsáki [52] (originally developed to describe CA1 hippocampal interneurons). The kinetics and maximal conductances, which are Hodgkin and Huxley style, are chosen so that the model displays two salient features of hippocampal and neocortical fast-spiking interneurons. The first being that the action potential is followed by a brief after-hyperpolarization, and the second that the model fires repetitive spikes at high frequencies. A plot of the response of this model to constant current injection is shown in Fig. 1. In the same figure we also show response of the aif model with the choice

$$f(v) = \begin{cases} (v - v_{\mathrm{s}}) & v > v_{\mathrm{s}} \\ -\alpha(v - v_{\mathrm{s}}) & v \leq v_{\mathrm{s}} \end{cases}, \qquad \alpha > 0. \tag{3}$$

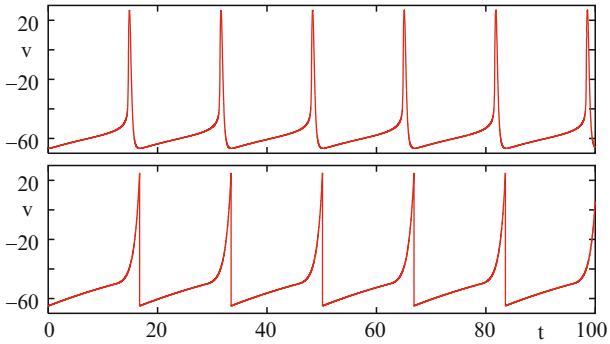

Fig. 1 *Top*: Periodic orbit in the Wang–Buzsáki model with constant current injection $I = 1$. *Bottom*: Periodic orbit in the aif model with $v_r = -65$, $v_s = -50$, $v_{th} = 25$, $\alpha = 0.03$, and $I = 1$

It is clear that an appropriately parametrized aif model can indeed capture the essential spike shape and frequency response of the more detailed biophysical model. Note that for accurate numerical computation of the spike times where $v \geq v_s$ (and solutions diverge as e^t) it is useful to consider the transformed variable $x = \ln(1 + v - v_s)$ and solve the dynamical system $\dot{x} = 1 + (I - 1)e^{-x}$ and then match to solutions with $v < v_s$.

Spike Adaptation

As well as supporting a tonic mode of spiking some interneurons have been reported to exhibit bursting [14, 38, 53]. With this in mind we show that by incorporating a form of spike adaptation [49] the aif model can exhibit both tonic and bursting behavior. For simplicity, we shall henceforth work with the explicit choice $f(v) = |v|$. In more detail we write

$$\dot{v} = |v| + I - a, \qquad \dot{a} = -a/\tau_a, \qquad \tau_a > 0, \tag{4}$$

subject to the usual IF reset mechanism as well as the adaptive step $a(T^m) \to a(T^m) + g_a/\tau_a$, for some $g_a > 0$. For sufficiently small g_a, the model fires tonically as shown in Fig. 2. Since the model is now a 2D (discontinuous) dynamical system it is also useful to view orbits in the (v, a) plane, where one can also plot the system nullclines, as shown in Fig. 3. For larger values of g_a, the model can also fire in a burst mode as shown in Fig. 4. The mechanism for this behavior is most easily understood in reference to the geometry of the phase-plane, as shown in Fig. 5. First consider that the dynamics after reset is such that the adaptive current is sufficiently strong so as to pull the trajectory toward the left-hand side of the voltage nullcline. If the separation of time-scales between the v and a variables is large (namely that

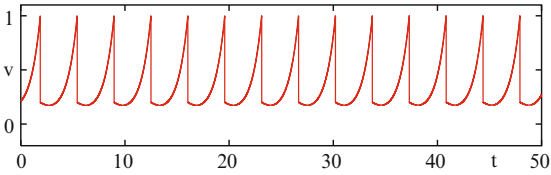

Fig. 2 Tonic firing in the aif model with spike adaptation. Here $\tau_a = 3$, $v_r = 0.2$, $v_{th} = 1$, $I = 0.1$, and $g_a = 0.75$

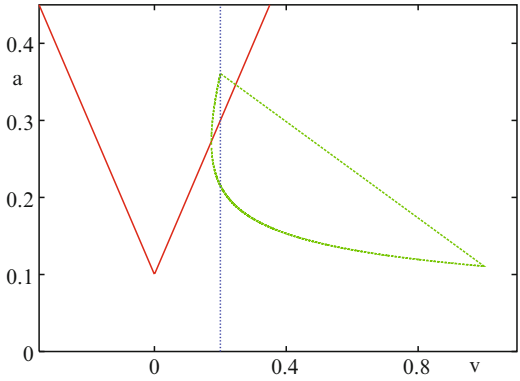

Fig. 3 A periodic orbit in the (v, a) plane corresponding to the tonic spiking trajectory shown in Fig. 2. Also shown is the voltage nullcline as well as the value of the reset

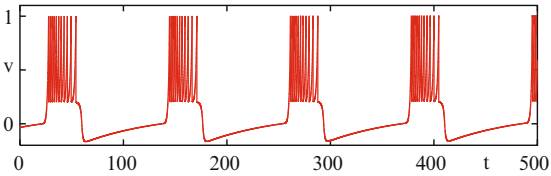

Fig. 4 Burst firing in the aif model with spike adaptation. Here $\tau_a = 75$, $v_r = 0.2$, $v_{th} = 1$, $I = 0.1$, and $g_a = 2$

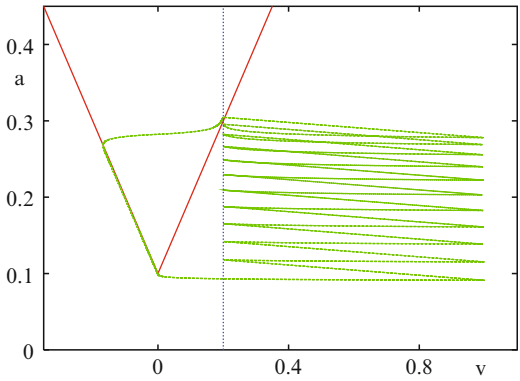

Fig. 5 A periodic orbit in the (v, a) plane corresponding to the bursting trajectory shown in Fig. 4

τ_a is large), then the trajectory will slowly track this nullcline ($a = I - v$) until it reaches $v = 0$, where there is a *switch* in the dynamics (from $f(v) = -v$ to $f(v) = +v$). After the switch the neuron is able to fire for as long as threshold can be reached – namely until a becomes so large as to preclude further firing. Thus, it is the negative feedback from the adaptive current that ultimately terminates a burst, and initiates a slow phase of subthreshold dynamics.

To solve the full nonlinear dynamical model, it is convenient to break the phase space into two regions separated by the line $v = 0$, so that in each region the dynamics (up to threshold and reset) is governed by a linear system. If we denote by v_+ and v_- the solution for $v > 0$ and $v < 0$, respectively, then variation of parameters gives us the closed form solution

$$v_\pm(t) = v_\pm(t_0)\mathrm{e}^{\pm(t-t_0)} + \int_{t_0}^{t} \mathrm{e}^{\mp(s-t)}[I - a(s)]\mathrm{d}s, \tag{5}$$

with initial data $v_\pm(t_0)$ and $t > t_0$. For example, considering the Δ-periodic tonic solution shown in Fig. 3, where $v > 0$ always, then we have that $a(t) = \overline{a}\mathrm{e}^{-t/\tau_a}$, with $\overline{a}$ determined self-consistently from $a(\Delta) + g_a/\tau_a = \overline{a}$, giving

$$\overline{a} = \frac{g_a}{\tau_a}\frac{1}{1 - \mathrm{e}^{-\Delta/\tau_a}}. \tag{6}$$

Hence, from (5), the voltage varies according to

$$v(t) = v_\mathrm{r}\mathrm{e}^t + I(\mathrm{e}^t - 1) - \frac{\overline{a}\tau_a}{1 + \tau_a}(\mathrm{e}^t - \mathrm{e}^{-t/\tau_a}). \tag{7}$$

The period is determined self-consistently by demanding that $v(\Delta) = v_\mathrm{th}$. A plot of the firing frequency $f = \Delta^{-1}$ as a function of g_a is shown in Fig. 6. From this we see that the frequency of tonic firing drops off with increasing adaptation, as expected. Note that one may also construct more complicated orbits (such as

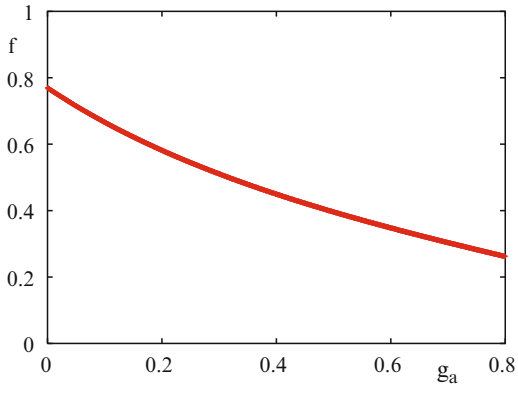

Fig. 6 Frequency of tonic firing as a function of the strength of adaptation g_a for the parameters of Fig. 2

tonic solutions which visit $v < 0$, period doubled tonic solutions, bursting states, etc.) using the ideas above. The main effort being in piecing together trajectories across $v = 0$.

Phase Response Curve

It is common practice to characterize a neuronal oscillator in terms of its phase response to a perturbation. This gives rise to the notion of a so-called phase response curve (PRC). For a detailed discussion of PRCs we refer the reader to [19, 20, 27]. Suffice to say that for a weak external perturbation, such that $(\dot{v}, \dot{a}) \to (\dot{v}, \dot{a}) + \epsilon(A_1(t), A_2(t))$, and ϵ small, then we can introduce a phase $\theta \in (0, 1)$ along a Δ-periodic orbit that evolves according to

$$\dot{\theta} = \frac{1}{\Delta} + \epsilon Q^T(A_1(t), A_2(t)). \tag{8}$$

The (vector) PRC, is given as $Q\Delta$, where Q obeys the so-called adjoint equation

$$\frac{\mathrm{d}Q}{\mathrm{d}t} = -DF^T(t)Q, \tag{9}$$

and $DF(t)$ is the Jacobian of the dynamical systems evaluated along the time-dependent orbit. To enforce the condition that $\dot{\theta} = 1/\Delta$ for $\epsilon = 0$ we must choose initial data for Q that guarantees $Q^T(\dot{v}, \dot{a}) = \Delta^{-1}$. For a continuous trajectory this normalization condition need only be enforced at a single point in time. However, for the aif model with adaptation there is a single discontinuity in the orbit (at reset) and so Q is not continuous. We therefore need to establish the conditions that ensure $Q(\Delta^+) = Q(0)$. Introducing components of Q as $Q = (q_1, q_2)$ this is equivalent to demanding continuity of $\mathrm{d}q_1/\mathrm{d}q_2$ at reset.

For the orbit given by (7) with $v > 0$ the Jacobian is simply the constant matrix

$$DF = \begin{bmatrix} 1 & -1 \\ 0 & -1/\tau_a \end{bmatrix}, \tag{10}$$

and the adjoint equation (9) may be solved in closed form as

$$q_1(t) = q_1(0)\mathrm{e}^{-t}, \qquad q_2(t) = q_2(0)\mathrm{e}^{t/\tau_a} + q_1(0)\frac{\tau_a}{1+\tau_a}[\mathrm{e}^{t/\tau_a} - \mathrm{e}^{-t}]. \tag{11}$$

The condition for continuity of $\mathrm{d}q_1/\mathrm{d}q_2$ at reset yields the relationship

$$\frac{q_2(0)}{q_1(0)} = \frac{q_2(\Delta)}{q_1(\Delta)} = -\frac{\tau_a}{1+\tau_a}, \tag{12}$$

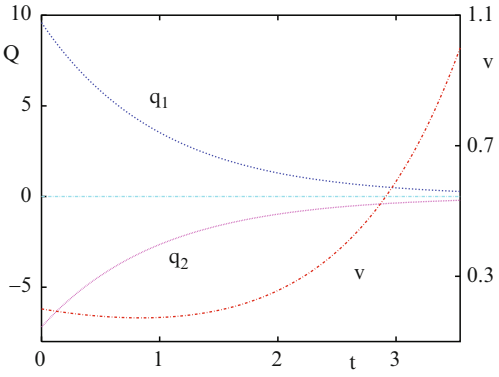

Fig. 7 Adjoint Q for the tonic spiking orbit shown in Fig. 3

whilst the normalization condition gives

$$q_1(0)[v_r + I - \overline{a}] - q_2(0)\frac{\overline{a}}{\tau_a} = \frac{1}{\Delta}. \tag{13}$$

The simultaneous solutions of (12) and (13) then gives the adjoint in the closed form

$$Q(t) = \frac{\kappa}{\Delta} e^{-t} \begin{bmatrix} 1 \\ -\tau_a/(1+\tau_a) \end{bmatrix}, \qquad t \in [0, \Delta), \tag{14}$$

and $\kappa = [v_r + I - \overline{a}\tau_a/(1+\tau_a)]^{-1}$. A plot of the adjoint for the tonic orbit (7) is shown in Fig. 7. Note that the orbit and PRC for other periodic solutions (crossing through $v = 0$) can be obtained in a similar fashion.

Gap-Junction Coupling

To model the direct gap-junction coupling between two cells, one labeled *post* and the other *pre*, we introduce an extra current to the right-hand side of equation (1) in the form

$$g_{\text{gap}}(v_{\text{pre}} - v_{\text{post}}), \tag{15}$$

where g_{gap} is the conductance of the gap junction. Indexing neurons in a network with the label $i = 1, \ldots, N$ and defining a gap-junction conductance strength between neurons i and j as g_{ij} means that neuron i experiences a drive of the form $N^{-1}\sum_{j=1}^{N} g_{ij}(v_j - v_i)$. For a phase locked state then $(v_i(t), a_i(t)) = (v(t - \phi_i\Delta), a(t - \phi_i\Delta))$, $(v(t), a(t)) = (v(t + \Delta), a(t + \Delta))$, (for some constant phases $\phi_i \in [0, 1)$) and we have N equations distinguished by the driving terms $N^{-1}\sum_{j=1}^{N} g_{ij}(v(t + (\phi_i - \phi_j)T) - v(t))$. For globally coupled networks with $g_{ij} = g$, maximally symmetric solutions describing synchronous, asynchronous, and cluster states

are expected to be generic [2]. Here we shall focus on asynchronous states defined by $\phi_i = i/N$. Such solutions are often called splay or merry-go-round states, since all oscillators in the network pass through some fixed phase at regularly spaced time intervals of Δ/N.

Existence of the Asynchronous State

Here we will focus on a globally coupled network in the large N limit. In this case, we have the useful result that network averages may be replaced by time averages. In this case, the coupling term for an asynchronous state becomes

$$\lim_{N\to\infty} \frac{1}{N}\sum_{j=1}^{N} v(t + j\Delta/N) = \frac{1}{\Delta}\int_0^{\Delta} v(t)\mathrm{d}t, \tag{16}$$

which is independent of both i and t. Hence, for an asynchronous state every neuron in the network is described by the same dynamical system, namely

$$\dot{v} = |v| - gv + I - a + gv_0, \qquad \dot{a} = -a/\tau_a, \tag{17}$$

where

$$v_0 = \frac{1}{\Delta}\int_0^{\Delta} v(t)\mathrm{d}t. \tag{18}$$

Once again we may use variation of parameters to obtain a closed form solution for the trajectory:

$$v_{\pm}(t) = v_{\pm}(t_0)\mathrm{e}^{\pm(t-t_0)/\tau_{\pm}} + \int_{t_0}^{t} \mathrm{e}^{\mp(s-t)/\tau_{\pm}}[I_g - a(s)]\mathrm{d}s, \tag{19}$$

where $\tau_{\pm} = 1/(1 \mp g)$ and $I_g = I + gv_0$. A self-consistent solution for the pair (Δ, v_0) is now obtained from the simultaneous solution of the two equations $v(\Delta) = v_{\mathrm{th}}$ and $v_0 = \Delta^{-1}\int_0^{\Delta} v(t)\mathrm{d}t$. For example an orbit with $v > 0$ is easily constructed and generates the two equations

$$v_{\mathrm{th}} = v_{\mathrm{r}}\mathrm{e}^{\Delta/\tau_+} + I_g\tau_+(\mathrm{e}^{\Delta/\tau_+} - 1) - \overline{a}\tau(\mathrm{e}^{\Delta/\tau_+} - \mathrm{e}^{-\Delta/\tau_a}), \tag{20}$$

$$v_0 = -I_g\tau_+ + \frac{1}{\Delta}\left\{\tau_+[\mathrm{e}^{\Delta/\tau_+} - 1][v_{\mathrm{r}} + I_g\tau_+ - \overline{a}\tau] + \overline{a}\tau\tau_a[1 - \mathrm{e}^{-\Delta/\tau_a}]\right\}, \tag{21}$$

where $1/\tau = 1/\tau_+ + 1/\tau_a$. A plot of (Δ, v_0) as a function of the gap strength g is shown in Fig. 8.

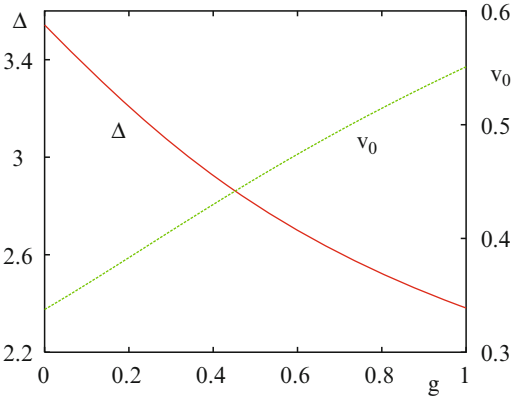

Fig. 8 Period Δ and constant mean field signal v_0 as a function of gap strength g. Other parameters as in Fig. 3 left

Stability of the Asynchronous State

Here we use a phase reduction technique, first developed by van Vreeswijk [48] for synaptic coupling, to study the stability of the asynchronous state. To do this we write the coupling term $N^{-1}\sum_{j=1}^{N} v_j(t)$ in a more convenient form for studying perturbations of the mean field, namely we write

$$\lim_{N\to\infty}\frac{1}{N}\sum_{j=1}^{N} v_j(t) = \lim_{N\to\infty}\frac{1}{N}\sum_{j=1}^{N}\sum_{m\in\mathbb{Z}} u(t-T_j^m), \tag{22}$$

where $T_j^m = m\Delta + j\Delta/N$. Here $u(t) = 0$ for $t < 0$ and is chosen such that $v(t) = \sum_{m\in\mathbb{Z}} u(t-m\Delta)$, ensuring that $v(t) = v(t+\Delta)$. For arbitrary values of the *firing-times* T_j^m the coupling term (22) is time-dependent, and we may write it in the form

$$E(t) = \int_0^\infty f(t-s)u(s)\mathrm{d}s, \qquad f(t) = \lim_{N\to\infty}\frac{1}{N}\sum_{j,m}\delta(t-T_j^m), \tag{23}$$

where we recognize $f(t)$ as a firing rate. We now consider perturbations of the mean field such that $E(t)$ (the average membrane voltage) is split into a stationary part (arising from the asynchronous state) and an infinitesimal perturbation. Namely we write $E(t) = v_0 + \epsilon(t)$, with small $\epsilon(t)$. Since this perturbation to the *asynchronous* oscillator defined by (17) is small we may use phase reduction techniques to study the stability of the asynchronous state.

In terms of a phase $\theta \in (0,1)$ along the asynchronous state we can write the evolution of this phase variable in response to a perturbation in the mean field as

$$\frac{\mathrm{d}\theta}{\mathrm{d}t} = \frac{1}{\Delta} + g\Gamma(\theta\Delta)\epsilon(t), \tag{24}$$

where Γ is the g-dependent voltage component of the adjoint for the asynchronous state. This can again be calculated in closed form using the techniques developed in section "Phase Response Curve," and takes the explicit form

$$\Gamma(t) = \frac{\kappa(g)}{\Delta} \mathrm{e}^{-t/\tau_+}, \tag{25}$$

where $\kappa(g) = [v_\mathrm{r}/\tau_+ + I_g - \overline{a}\tau_a/(1+\tau_a)]^{-1}$. In fact we need to treat N phase variables θ_i, each described by an equation of the form (24), which are coupled by the dependence of $\epsilon(t)$ on these variables. To make this more explicit we write

$$\epsilon(t) = \int_0^\infty \delta f(t-s) u(s) \mathrm{d}s, \tag{26}$$

and use a phase density description to calculate the dependence of the perturbed firing rate δf on the phases. We define a phase density function as the fraction of neurons in the interval $[\theta, \theta + \mathrm{d}\theta]$ namely $\rho(\theta, t) = N^{-1} \sum_j \delta(\theta_j(t) - \theta)$. Introducing the flux $J(\theta, t) = \rho(\theta, t)\dot{\theta}$, we have the continuity equation

$$\frac{\partial \rho}{\partial t} = -\frac{\partial J}{\partial \theta}, \tag{27}$$

with boundary condition $J(1,t) = J(0,t)$. The firing rate is the flux through $\theta = 1$, so that $f(t) = J(1,t)$. In the asynchronous state the phase density function is independent of time. Considering perturbations around this state, $(\rho, J) = (1, \Delta^{-1})$, means writing $\rho(\theta, t) = 1 + \delta\rho(\theta, t)$, with a corresponding perturbation of the flux that takes the form $\delta J(\theta, t) = \delta\rho(\theta, t)/\Delta + g\Gamma(\theta\Delta)\epsilon(t)$. Differentiation of $\delta J(\theta, t)$ gives the partial differential equation

$$\partial_t \delta J(\theta, t) = -\frac{1}{\Delta} \partial_\theta \delta J(\theta, t) + g\Gamma(\theta\Delta)\epsilon'(t), \tag{28}$$

where

$$\epsilon(t) = \int_0^\infty u(s) \delta J(1, t-s) \mathrm{d}s. \tag{29}$$

Assuming a solution of the form $\delta J(\theta, t) = \mathrm{e}^{\lambda t} \delta J(\theta)$, gives

$$\epsilon(t) = \delta J(1) \mathrm{e}^{\lambda t} \widetilde{u}(\lambda), \tag{30}$$

where $\widetilde{u}(\lambda) = \int_0^\infty u(t) \mathrm{e}^{-\lambda t} \mathrm{d}t$. In this case $\epsilon'(t) = \lambda\epsilon(t)$. Equation (28) then reduces to the ordinary differential equation

$$\frac{\mathrm{d}}{\mathrm{d}\theta} \delta J(\theta) \mathrm{e}^{\lambda\Delta\theta} = g\lambda\Delta\Gamma(\theta\Delta) \delta J(1) \widetilde{u}(\lambda) \mathrm{e}^{\lambda\Delta\theta}. \tag{31}$$

Integrating (31) from $\theta = 0$ to $\theta = 1$ and using the fact that $\delta J(1) = \delta J(0)$ yields an implicit equation for λ in the form $\mathcal{E}(\lambda) = 0$, where

$$\mathcal{E}(\lambda) = \mathrm{e}^{\lambda\Delta} - 1 - g\lambda\Delta\widetilde{u}(\lambda)\int_0^1 \Gamma(\theta\Delta)\mathrm{e}^{\lambda\theta\Delta}\mathrm{d}\theta. \tag{32}$$

We see that $\mathcal{E}(0) = 0$ so that $\lambda = 0$ is always an eigenvalue. Writing $\lambda = \nu + i\omega$ then the pair (ν, ω) may be found by the simultaneous solution of $\mathcal{E}_{\mathrm{R}}(\nu, \omega) = 0$ and $\mathcal{E}_{\mathrm{I}}(\nu, \omega) = 0$, where $\mathcal{E}_{\mathrm{R}}(\nu, \omega) = \mathrm{Re}\,\mathcal{E}(\nu + i\omega)$ and $\mathcal{E}_{\mathrm{I}}(\nu, \omega) = \mathrm{Im}\,\mathcal{E}(\nu + i\omega)$.

For the adjoint calculated given by (25) a simple calculation gives

$$\int_0^1 \Gamma(\theta\Delta)\mathrm{e}^{\lambda\theta\Delta}\mathrm{d}\theta = \frac{\kappa(g)}{\Delta}\frac{1}{\Delta}\frac{\mathrm{e}^{\Delta(\lambda-1/\tau_+)} - 1}{(\lambda - 1/\tau_+)}. \tag{33}$$

For the calculation of $\widetilde{u}(\lambda)$ we use the result that $\int_0^\infty u(t)\mathrm{e}^{-\lambda t}\mathrm{d}t = \int_0^\Delta v(t+s)\mathrm{e}^{-\lambda t}\mathrm{d}t$, for some arbitrary time-translation $s \in (0, \Delta)$, with $v(t)$ the splay solution, defined for $t \in (0, \Delta)$. In contrast to the calculations in [12] for continuous periodic orbits, those of the aif model are discontinuous and so one must carefully treat this extra degree of freedom. Since we do not a priori know the phase of the signal $v(t)$ with respect to the time origin of the oscillator model we simply average over all possible phases and write

$$\widetilde{u}(\lambda) = \frac{1}{\Delta}\int_0^\Delta \left\{ \int_0^\Delta v(t+s)\mathrm{e}^{-\lambda t}\mathrm{d}t \right\} \mathrm{d}s. \tag{34}$$

For the splay solution of section "Existence of the Asynchronous State," a short calculation gives

$$\begin{aligned}\frac{\widetilde{u}(\lambda)}{\mathrm{e}^{\lambda\Delta} - 1} = {} & \frac{v_{\mathrm{r}} + I_g\tau_+ - \overline{a}\tau}{\lambda - 1/\tau_+}\frac{\tau_+}{\Delta}(\mathrm{e}^{-\Delta(\lambda-1/\tau_+)} - \mathrm{e}^{-\lambda\Delta}) - I_g\tau_+\frac{\mathrm{e}^{-\lambda\Delta}}{\lambda} \\ & - \frac{\overline{a}\tau}{\lambda + 1/\tau_a}\frac{\tau_a}{\Delta}(\mathrm{e}^{-\Delta(\lambda+1/\tau_a)} - \mathrm{e}^{-\lambda\Delta}), \qquad \mathrm{Re}\,\lambda < 1/\tau_+. \end{aligned} \tag{35}$$

For $\lambda \in \mathbb{R}$ the condition for an eigenvalue to cross through zero from below is equivalent to the occurrence of a double zero of $\mathcal{E}(\lambda)$ at $\lambda = 0$. However, it is easy to show that $\mathcal{E}'(0) \neq 0$ so that no instabilities can arise in this fashion. Examples of the spectrum obtained from the zeros of $\mathcal{E}(\lambda)/(\mathrm{e}^{\lambda\Delta} - 1)$ are shown in Fig. 9 (the remaining zeros of $\mathcal{E}(\lambda)$ being at $\lambda\Delta = 2\pi i n, n \in \mathbb{Z}$).

Here we see that for fixed g and increasing g_a, a pair of complex conjugate eigenvalues crosses through the imaginary axis at a nonzero value of ω. This signals the onset of a dynamic instability, which is more easily quantified with the aid of Fig. 10 which tracks the first pair (ν, ω) to pass through $\nu = 0$ as a function of g_a. Until now we have assumed that the splay state exists for all parameters of choice. However, because the underlying model is described by a discontinuous flow then

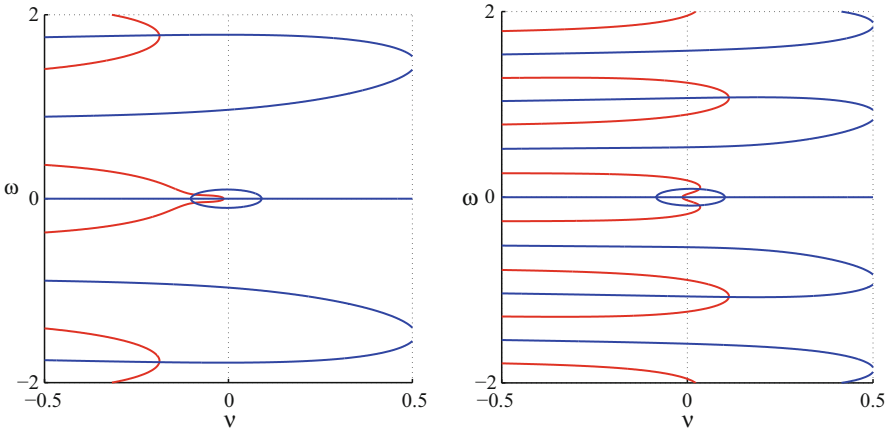

Fig. 9 Spectrum for the asynchronous state. Eigenvalues are at the positions where the red and blue curves intersect. Parameters as in Fig. 4 with $g = 0.5$. *Left*: $g_a = 1.5$, with $(\Delta, v_0) = (4.0575, 0.46685)$. *Right*: $g_a = 2.5$, with $(\Delta, v_0) = (6.6757, 0.39433)$. Note the unstable mode with $\omega \sim \pm 1$ in the right-hand figure.

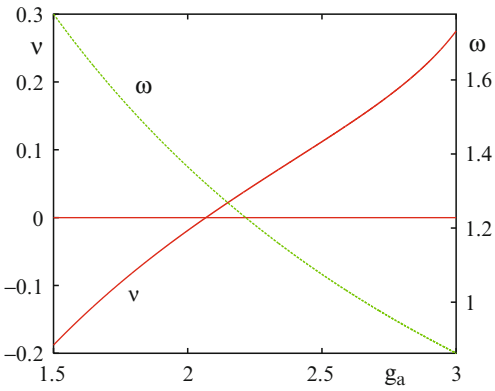

Fig. 10 A plot of (v, ω), where $\mathcal{E}(v + i\omega) = 0$, as a function of g_a, with other parameters as in Fig. 9. Note the bifurcation at $g_a \sim 2.1$, where v crosses zero from below with a nonzero value of ω.

there is also the possibility that a nonsmooth bifurcation can occur. For example a splay state with $v \geq 0$ may tangentially intersect the surface $v = 0$, where there is a switch in the dynamics for v. In this case, a new orbit will emerge that can either be tonic or bursting. The conditions defining this nonsmooth bifurcation are $v(t^*) = 0$ and $\dot{v}(t^*) = 0$ for some $t^* \in (0, \Delta)$. For the splay state considered here, we find that a dynamic instability, defined by $\mathcal{E}(i\omega) = 0$, is always met before the onset of a nonsmooth bifurcation.

By tracking the bifurcation point $v = 0$ in parameter space it is possible to map out those regions where the asynchronous state is stable. We do this in Fig. 11 which basically shows that if an asynchronous state is stable for fixed (g, τ_a) then it can always be destabilized by increasing g_a beyond some critical value.

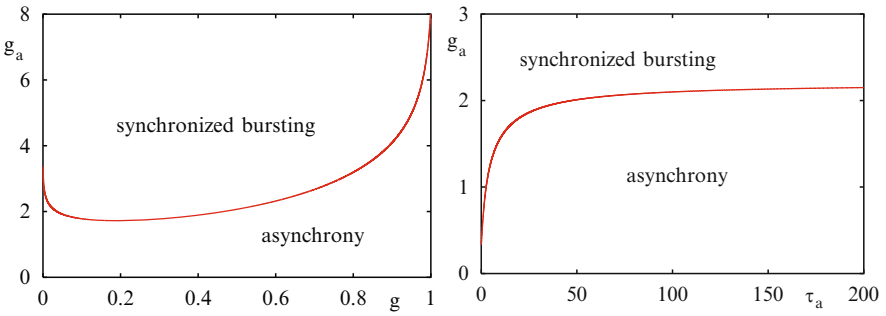

Fig. 11 Curves showing solutions of $\mathcal{E}(i\omega) = 0$ obtained by tracking the bifurcation point in Fig. 10. Parameters as in Fig. 9. *Left*: $\tau_a = 75$. *Right*: $g = 0.5$. Beyond an instability point of the asynchronous solution one typically sees the emergence of synchronized bursting states, as shown in Fig. 12

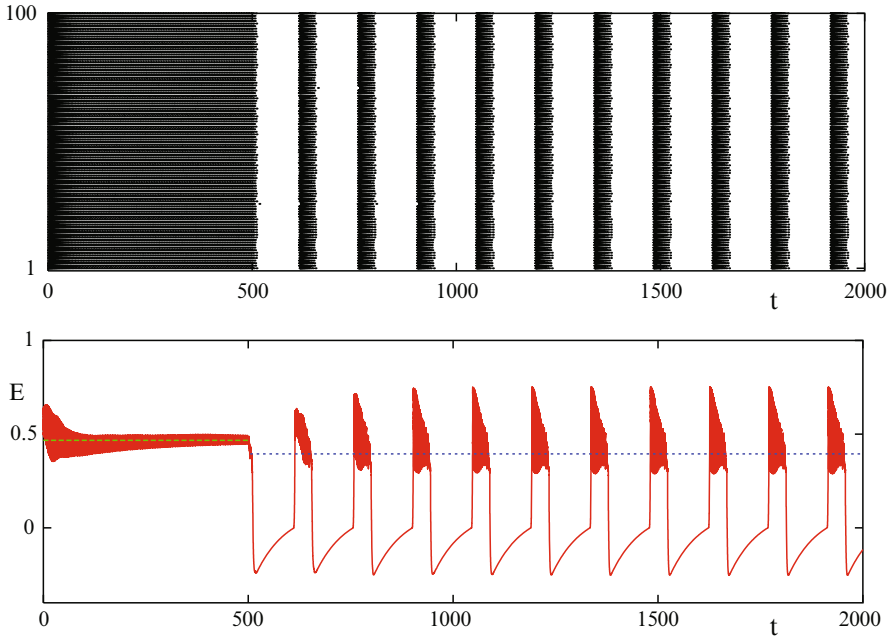

Fig. 12 A plot showing an instability of the asynchronous state in a network with $N = 100$ neurons, starting from random initial conditions. Here g_a is switched from the value in Fig. 9 left (asynchronous state stable) to that in Fig. 9 right (asynchronous state unstable) at $t = 500$. Note the emergence of a synchronized bursting state. The *lower plot* shows the time variation of the mean-field signal $E(t) = N^{-1}\sum_{i=1}^{N} v_i(t)$, as well as the value of v_0 – the mean field signal for the asynchronous state (*dashed and dotted lines*). Parameters as in Fig. 9

To determine the types of solutions that emerge beyond the instability borders we have performed direct numerical simulations. Not only do these confirm the correctness of our bifurcation theory, they show that a dominant emergent solution is a bursting mode in which neurons are synchronized at the level of their firing rates, but not at the level of individual spikes (within a burst). An example of a network state that switches from asynchronous tonic spiking to synchronized bursting with a switch in g_a across the bifurcation point is shown in Fig. 12. Here we plot both a raster diagram showing spike times as well as the mean field signal $E(t) = N^{-1} \sum_{i=1}^{N} v_i(t)$ for a network of 100 neurons. Interestingly the plot of the mean field signal suggests that bursting terminates roughly at the point where it reaches the value of v_0 for the unstable asynchronous orbit.

Discussion

In this chapter, we have shown how the absolute integrate-and-fire model is ideally suited for the theoretical study of gap-junction coupled networks. One such network where theory may help shed further light on function is that of the inferior olivary nucleus, which has extensive electrotonic coupling between dendrites. Chorev et al. [11] have shown that in vivo intracellular recordings from olivary neurons (of anesthetized rats) exhibit subthreshold oscillations of membrane voltage, organized in epochs, lasting from half a second to several seconds. If recorded, spikes were locked to the depolarized phase of these subthreshold oscillations. Thus it is of interest to probe the way in which neurons supporting both subthreshold oscillations and spikes use gap-junction coupling to coordinate spatiotemporal patterns for holding and then transferring rhythmic information to cerebellar circuits [50]. The techniques we have developed here are ideally suited to this task.

At the level of the single neuron we have shown how to construct both the periodic orbit and the phase response curve. This is particularly useful for the development of a weakly coupled oscillator theory for network studies, for both gap and synaptic coupling, as in the work of Kazanci and Ermentrout [31]. However, we have chosen here to instead pursue a strongly coupled network analysis. The tractability of the chosen model has allowed the explicit calculation of the asynchronous state, including the determination of its linear stability, in large globally gap-junction coupled networks. In the presence of a simple form of spike adaptation we have quantified a bifurcation from asynchrony to synchronized bursting. Interestingly, burst synchronization has been observed in both cell cultures and brain areas such as the basal ganglia. For a review of experiments and theory relating to burst synchronization we refer the reader to the article by Rubin [44]. One natural progression of the work in this chapter would be to analyze the properties of bursting in more detail, and in particular the synchronization properties of bursts relating to both gap and synaptic parameters. Techniques for doing this are relatively underdeveloped as compared to those for studying synchronized tonic spiking. However, it is well to point out the work of Izhikevich [29], de Vries and Sherman [13], and

Matveev et al. [39] in this area, as well as more recent numerical studies [43, 45]. The development of such a theory is especially relevant to so-called *neural signatures*, which consist of cell-specific spike timings in the bursting activity of neurons. These very precise intra-burst firing patterns may be quantified using computational techniques discussed in [33]. We refer the reader to [34] for a recent discussion of neural signatures in the context of the pyloric central pattern generator of the crustacean stomatogastric ganglion (where gaps are known to play a role in rhythm generation).

From a biological perspective it is important to emphasize that gaps are not the static structures that we have suggested here by treating gap strength as a single parameter. Indeed the connexin channels that underlie such junctions are dynamic and are in fact modulated by the voltage across the membrane. Baigent et al. [3] have developed a model of the dependency between the cell potentials and the *state* of the gap junctions. In this context the state of an individual channel corresponds to the conformation of the two connexons forming the pore. Of the four possible states (both open, both closed, or one open, and one closed), the scenario where both are closed is ignored. Because each cell–cell junction is composed of many channels, the state of the junction is determined by the distribution of channels amongst the three different states. Thus it would be interesting to combine the model we have presented here with this channel model and explore the consequences for coherent network behavior. Another form of gap-junction modulation can be traced to cannabinoids. Gap-junction coupling can be found among irregular spiking GABAergic interneurons that express cannabinoid receptors [23]. Interestingly, the potentiation of such coupling by cannabinoids has recently been reported [10]. All of the above are topics of current investigation and will be reported upon elsewhere.

Acknowledgments We would like to thank Bard Ermentrout for bringing our attention to the work of Karbowski and Kopell.

References

1. A. V. Alvarez, C. C. Chow, E. J. V. Bockstaele, and J. T. Williams. Frequency-dependent synchrony in locus ceruleus: Role of electrotonic coupling. *Proceedings of the National Academy of Sciences*, 99(6):4032–4036, 2002.
2. P. Ashwin and J. W. Swift. The dynamics of n weakly coupled identical oscillators. *Journal of Nonlinear Science*, 2:69–108, 1992.
3. S. Baigent, J. Stark, and A. Warner. Modelling the effect of gap junction nonlinearities in systems of coupled cells. *Journal of Theoretical Biology*, 186:223–239, Jan 1997.
4. M. Beierlein, J. R. Gibson, and B. W. Connors. A network of electrically coupled interneurons drives synchronized inhibition in neocortex. *Nature Neuroscience*, 3(9):904–910, 2000.
5. M. V. L. Bennet and R. S. Zukin. Electrical coupling and neuronal synchronization in the mammalian brain. *Neuron*, 41:495–511, 2004.
6. M. Bennett, J. Contreras, F. Bukauskas, and J. Sáez. New roles for astrocytes: gap junction hemichannels have something to communicate. *Trends in Neurosciences*, 26:610–617, 2003.

7. M. Blatow, A. Rozov, I. Katona, S. G. Hormuzdi, A. H. Meyer, M. A. Whittington, A. Caputi, and H. Monyer. A novel network of multipolar bursting interneurons generates theta frequency oscillations in neocortex. *Neuron*, 38(5):805–817, 2003.
8. C. Bou-Flores and A. J. Berger. Gap junctions and inhibitory synapses modulate inspiratory motoneuron synchronization. *Journal of Neurophysiology*, 85(4):1543–1551, 2001.
9. G. Buzsaki. *Rhythms of the Brain*. Oxford University Press, Inc., USA, 2006.
10. R. Cachope, K. Mackie, A. Triller, J. O'Brien, and A. E. Pereda. Potentiation of electrical and chemical synaptic transmission mediated by endocannabinoids. *Neuron*, 56(6):1034–1047, 2007.
11. E. Chorev, Y. Yarom, and I. Lampl. Rhythmic episodes of subthreshold membrane potential oscillations in the rat inferior olive nuclei *in vivo*. *The Journal of Neuroscience*, 27:5043–5052, 2007.
12. S. Coombes. Neuronal networks with gap junctions: a study of piece-wise linear planar neuron models. *SIAM Journal on Applied Dynamical Systems*, 7:1101–1129, 2008.
13. G. de Vries and A. Sherman. *Bursting: The Genesis of Rhythm in the Nervous System*, chapter Beyond synchronization: modulatory and emergent effects of coupling in square-wave bursting. World Scientific, 2005.
14. J. Deuchars and A. M. Thomson. Single axon fast inhibitory postsynaptic potentials elicited by a sparsely spiny interneuron in rat neocortex. *Neuroscience*, 65(4):935–942, 1995.
15. S. Dhein and J. S. Borer, editors. *Cardiovascular Gap Junctions (Advances in Cardiology)*. S Karger AG, 2006.
16. A. Draguhn, R. D. Traub, D. Schmitz, and J. G. Jefferys. Electrical coupling underlies high-frequency oscillations in the hippocampus in vitro. *Nature*, 394(6689):189–192, 1998.
17. F. E. Dudek. Gap junctions and fast oscillations: a role in seizures and epileptogenesis? *Epilepsy Currents*, 2:133–136, 2002.
18. B. Ermentrout. Gap junctions destroy persistent states in excitatory networks. *Physical Review E*, 74:031918(1–8), 2006.
19. G. B. Ermentrout and N. Kopell. Oscillator death in systems of coupled neural oscillators. *SIAM Journal on Applied Mathematics*, 50:125–146, 1990.
20. G. B. Ermentrout and N. Kopell. Multiple pulse interactions and averaging in systems of coupled neural oscillators. *Journal of Mathematical Biology*, 29:195–217, 1991.
21. T. F. Freund. Interneuron diversity series: rhythm and mood in perisomatic inhibition. *Trends in Neurosciences*, 26(9):489–495, 2003.
22. E. J. Furshpan and D. D. Potter. Mechanism of nerve-impulse transmission at a crayfish synapse. *Nature*, 180:342–343, 1957.
23. M. Galarreta, F. Erdelyi, G. Szabo, and S. Hestrin. Electrical coupling among irregular-spiking GABAergic interneurons expressing cannabinoid receptors. *Journal of Neuroscience*, 24:9770–9778, 2004.
24. M. Galarreta and S. Hestrin. A network of fast-spiking cells in the neocortex connected by electrical synapses. *Nature*, 402(6757):72–75, 1999.
25. J. R. Gibson, M. Beierlein, and B. W. Connors. Two networks of electrically coupled inhibitory neurons in neocortex. *Nature*, 402(6757):75–79, 1999.
26. J. R. Gibson, M. Beierlein, and B. W. Connors. Functional properties of electrical synapses between inhibitory interneurons of neocortical layer 4. *Journal of Neurophysiology*, 93:467–480, 2005.
27. F. C. Hoppensteadt and E. M. Izhikevich. *Weakly Connected Neural Networks*. Number 126 in Applied Mathematical Sciences. Springer-Verlag, New York, 1997.
28. S. G. Hormuzdi, M. A. Filippov, G. Mitropoulou, H. Monyer, and R. Bruzzone. Electrical synapses: a dynamic signaling system that shapes the activity of neuronal networks. *Biochimica et Biophysica Acta*, 1662:113–137, 2004.
29. E. M. Izhikevich. Synchronization of elliptic bursters. *SIAM Review*, 43:315–344, 2001.
30. J. Karbowski and N. Kopell. Multispikes and synchronization in a large-scale neural network with delays. *Neural Computation*, 12:1573–1606, 2000.
31. F. G. Kazanci and B. Ermentrout. Pattern formation in an array of oscillators with electrical and chemical coupling. *SIAM Journal on Applied Mathematics*, 67:512–529, 2007.

32. N. Kopell and B. Ermentrout. Chemical and electrical synapses perform complementary roles in the synchronization of interneuronal networks. *Proceedings of the National Academy of Sciences USA*, 101:15482–15487, 2004.
33. L. F. Lago-Fernández. Spike alignment in bursting neurons. *Neurocomputing*, 70:1788–1791, 2007.
34. R. Latorre, F. B. Rodríguez, and P. Varona. Neural signatures: multiple coding in spiking-bursting cells. *Biological Cybernetics*, 95:169–183, 2006.
35. T. J. Lewis and J. Rinzel. Dynamics of spiking neurons connected by both inhibitory and electrical coupling. *Journal of Computational Neuroscience*, 14:283–309, 2003.
36. J. G. Mancilla, T. J. Lewis, D. J. Pinto, J. Rinzel, and B. W. Connors. Synchronization of electrically coupled pairs of inhibitory interneurons in neocortex. *The Journal of Neuroscience*, 27:2058–2073, 2007.
37. P. Mann-Metzer and Y. Yarom. Electrotonic coupling interacts with intrinsic properties to generate synchronized activity in cerebellar networks of inhibitory interneurons. *Journal of Neuroscience*, 19(9):3298–3306, 1999.
38. H. Markram, M. Toledo-Rodriguez, Y. Wang, A. Gupta, G. Silberberg, and C. Wu. Interneurons of the neocortical inhibitory system. *Nature Reviews Neuroscience*, 5:793–807, 2004.
39. V. Matveev, A. Bose, and F. Nadim. Capturing the bursting dynamics of a two-cell inhibitory network using a one-dimensional map. *Journal of Computational Neuroscience*, 23:169–187, 2007.
40. H. B. Michelson and R. K. Wong. Synchronization of inhibitory neurones in the guinea-pig hippocampus in vitro. *Journal of Physiology*, 477(Pt 1):35–45, 1994.
41. B. Pfeuty, D. Golomb, G. Mato, and D. Hansel. Inhibition potentiates the synchronizing action of electrical synapses. *Frontiers in Computational Neuroscience*, 1(Article 8), 2007.
42. B. Pfeuty, G. Mato, D. Golomb, and D. Hansel. Electrical synapses and synchrony: the role of intrinsic currents. *The Journal of Neuroscience*, 23:6280–6294, 2003.
43. S. Postnova, K. Voigt, and H. A. Braun. Neural synchronization at tonic-to-bursting transitions. *Journal of Biological Physics*, 33:129–143, 2007.
44. J. E. Rubin. Burst synchronization. *Scholarpedia*, 2(10):1666, 2007.
45. Y. Shen, Z. Hou, and H. Xin. Transition to burst synchronization in coupled neuron networks. *Physical Review E*, 77:031920(1–5), 2008.
46. A. Sherman and J. Rinzel. Rhythmogenic effects of weak electrotonic coupling in neuronal models. *Proceedings of the National Academy of Sciences USA*, 89:2471–2474, 1992.
47. G. Tamas, E. H. Buhl, A. Lorincz, and P. Somogyi. Proximally targeted GABAergic synapses and gap junctions synchronize cortical interneurons. *Nature Neuroscience*, 3(4):366–371, 2000.
48. C. van Vreeswijk. Analysis of the asynchronous state in networks of strongly coupled oscillators. *Physical Review Letters*, 84:5110–5113, 2000.
49. C. van Vreeswijk and D. Hansel. Patterns of synchrony in neural networks with spike adaptation. *Neural Computation*, 13:959–992, Jan 2001.
50. P. Varona, C. Aguirre, J. J. Torres, H. D. I. Abarbanel, and M. I. Rabinovich. Spatio-temporal patterns of network activity in the inferior olive. *Neurocomputing*, 44–46:685–690, 2002.
51. J. L. P. Velazquez and P. L. Carlen. Gap junctions, synchrony and seizures. *Trends in Neurosciences*, 23:68–74, 2000.
52. X. J. Wang and G. Buzsaki. Gamma oscillation by synaptic inhibition in a hippocampal interneuronal network. *Journal of Neuroscience*, 16:6402–6413, 1996.
53. J. J. Zhu, D. J. Uhlrich, and W. W. Lytton. Burst firing in identified rat geniculate interneurons. *Neuroscience*, 91:1445–1460, 1999.